Modulating the Steric, Electronic and Catalytic Properties of Cp* Ruthenium Half-sandwich Complexes with β-diketiminato Ligands

Supporting Information

Andrew D. Phillips,[a,c] Katrin Thommes,[a] Rosario Scopelliti,[a] Claudio Gandolfi,[b] Martin Albrecht,[b,c] Kay Severin[a], Dominique F. Schreiber[c] and Paul J. Dyson[a]*

a. Institut des Sciences et Ingénierie Chimiques, Ecole Polytechnique Fédérale de Lausanne (EPFL), CH-1015 Lausanne, Switzerland.
b. Department of Chemistry, University of Fribourg, Chemin du Musée 9, CH-1700 Fribourg, Switzerland.
c. School of Chemistry and Chemical Biology, University College Dublin, Belfield, Dublin 4, Ireland.

Table of Contents

S1.1: *Comparison of electronic structure between Ru^{III} and Ru^{II} β-diketiminate complexes bearing the auxiliary Cp* ligand*

To gain insight towards the electronic and bonding structure of the β-diketiminato-Cp* Ru^{III} and Ru^{II} complexes with and without chlorine, four representative compounds were modelled using density functional theory (DFT) methods, specifically the B3LYP level of theory, complexes **7** and **11** bearing electron donating groups on the β-diketiminate and **13** and **17** with multiple CF_3 substitution on the β-diketiminate ligand. In all cases, full methyl substitution on the η^5-cyclopentyldienyl ligand was employed. The models were optimized using the highest symmetry group point, which in most cases, was C_s. Each calculated model was verified to be minimum point on the potential energy surface as indicated by the calculation of null imagery frequencies. Complex **11**, however, in C_s symmetry featured one imaginary frequency, and thus slight rotation of the Cp* group about the centroid-Ru axis, resulting in C_1 symmetry model was found to be the true minimum with no imagery frequencies. Comparison of the optimized model geometries with the obtained solid-state structures determined from single X-ray diffraction techniques, show good agreement for the β-diketiminate ligand component. However, as is often observed in DFT methods, metal-ligand bond lengths are greater in the model cases in contrast to experimental values. Importantly, the geometric-based trends in bond lengths and angles parameters are consistent between complexes bearing electron-donating and electron withdrawing substituents.

In particular, key parameters such as the Ru-N bond length, Ru-Cp* distance and N-Ru-N bond angle are reproduced with the same trend between both sets of complexes, *i.e.,* chloro-substituted Ru^{III} and unsaturated Ru^{II} complexes. A comparison of important metric parameters is shown in Table S1. The contrast between employing an electron donating or an electron withdrawing β-diketiminate ligand can be observed as inducing a number of different electronic effects including bond polarization and charge transfer. Such effects considerably alter other metal ligand interactions including the Cl and Cp* groups. An analysis of the Mayer bond indices (BDI), provides a relative, normalized, measure of the electron population in a bond,[1] with two, three or multiple atomic centers. Table S2 shows the important trends among the four selected model complexes. The BDI analyses reveal several important features and correlates with the observed geometry, in terms of bond length. The Ru-N bonds are weakened in the Ru^{III} complexes compared to the corresponding Ru^{II} series. Interestingly, in the Ru^{III} complexes the inclusion of α-CF_3 groups depletes electron density of the adjoining N-C_α and C_α-C_β bonds, which in turn results in weakened Ru-N bonds.

Table S1: Comparison of key metric parameters; bond lengths (Å), bond angles (°) for DFT calculated models and solid structure derived from X-ray diffraction data for two selected Ru^{III} complexes **7** and **11**, and two selected Ru^{II} complexes **13** and **17**.

Parameter	**7** model	**7** exp.	**11** model	**11** exp.	**13** model	**13** exp.	**17** model	**17** exp.
Ru-N	2.116	2.075(2) 2.089(2)	2.099	2.071(3) 2.070(3)	2.091	2.071(2) 2.060(3)	2.075	2.055(6) 2.056(6) 2.035(6) 2.025(6)
N-C_{ipso}	1.440	1.452(4) 1.453(4)	1.434	1.443(4) 1.440(4)	1.438	1.447(4) 1.452(4)	1.437	1.463(10) 1.437(9) 1.464(9) 1.455(9)
N-C_{α}	1.335	1.342(4) 1.347(4)	1.332	1.324(4) 1.329(4)	1.346	1.349(4) 1.348(4)	1.345	1.334(10) 1.367(10) 1.353(10) 1.372(10)
C_{α}-C_{β}	1.404	1.402(5) 1.399(5)	1.395	1.390(5) 1.395(6)	1.398	1.393(5) 1.396(5)	1.393	1.404(11) 1.388(12) 1.379(12) 1.373(12)
Ru-Cp*[a]	1.949	1.890(1)	1.954	1.881(2)	1.857	1.819(1)	1.862	1.828(3) 1.821(3)
Ru-Cl	2.462	2.461(1)	2.444	2.430(1)	-	-	-	-
N-Ru-N	87.97	87.5(1)	89.68	89.7(1)	87.99	87.2(1)	89.21	89.6(3) 89.3(2)
Ru-N-C_{ipso}	120.18	120.8(2) 119.7(2)	116.09	115.4(2) 116.5(2)	117.51	116.8(2) 117.0(2)	116.07	117.0(5) 116.6(4) 117.0(4) 117.9(4)
Ru-N-C_{α}	123.62	124.0(2) 125.2(2)	124.65	125.6(2) 125.7(2)	127.86	128.9(2) 129.3(2)	126.43	126.9(5) 126.7(5) 127.3(5) 127.6(5)
N-C_{α}-C_{β}	123.34	123.7(3) 123.5(3)	125.78	125.5(4) 125.2(3)	123.93	123.3(3) 123.1(3)	125.14	125.1(7) 124.2(7) 124.0(7) 123.2(7)
C_{α}-C_{β}-C_{α}	128.28	127.4(3)	127.95	127.6(3)	128.53	128.1(3)	127.49	127.4(7) 128.6(7)

Note: (a) Represents the distance between the Ru center and the centroid point of the Cp* ligand.

Table S2: Mayer bond indices[1] (MBI) obtained from calculated DFT models.

	Complex			
Bond	**7**	**11**	**13**	**17**
N-Ru	0.518	0.498	0.537	0.559
Avg. C_{Cp^*}-Ru	0.388	0.390	0.474	0.472
N-C_{α}	1.383	1.379	1.342	1.316
N-C_{ipso}	0.963	0.916	0.960	0.914
C_{α}-C_{β}	1.361	1.329	1.381	1.345
C_{α}-CR_3	1.002	0.956	1.000	0.961
Ru-Cl	0.819	0.907	n/a	n/a

However, in the case of the Ru^{II}, the α-CF_3 groups readily deplete N=C_α and C_α-C_β bond electron density, but the Ru-N bonds are strengthened in accordance with shortened bond length. The interaction between the Cp* and Ru centers is also strengthened for the Ru^{II} complexes compared to the oxidized analogs.

One particular interesting question is the degree of electron transfer between each of the ligands, i.e., β-diketiminate and the Cp* and the metal center. In recent years, a number of post-analysis MO analysing tools have been developed to divide and isolate the various contributions which including ligand to metal donation and metal to ligand back donation. Charge decomposition analysis (CDA) uses a fragment isolation approach to deconvolute contributions originating from electron transfer between fragments. Therefore, using the program AOMIX,[2] the CDA method developed by Frenking *et al*.[3] was performed on each of the model complexes for the two fragment combinations β-diketiminate↔Ru(Cp)*/Ru(Cp)*Cl and Cp*↔Ru(β-diketiminate)/Ru(β-diketiminate)Cl, and for the Ru^{III} containing species, an additional interaction between Cp*Ru(β-diketiminate)↔Cl^- was examined. The resulting values provides the quantity of electron density transferred between fragments, the net electron donation is also calculated, see Table S3.

Table S3: Calculated electron density donation between molecular fragments within complexes **7**,**11**, **13** and **17**.

	Complex			
Fragment	**7 Ru^{III}**	**11 Ru^{III}**	**13 Ru^{II}**	**17 Ru^{II}**
β-diketiminate →Ru(Cp*)/Ru(Cp*)Cl	0.759	0.678	0.450	0.415
β-diketiminate←Ru(Cp*)/Ru(Cp*)Cl	0.097	0.079	0.066	0.071
Cp*→Ru(β-diketiminate)/RuCl(β-diketiminate)	0.935	0.891	0.544	0.519
Cp*←Ru(β-diketiminate)/RuCl(β-diketiminate)	0.258	0.272	0.206	0.211
Cp*Ru(β-diketiminate)→Cl^-	0.022	0.026	-	-
Cp*Ru(β-diketiminate)←Cl^-	0.696	0.681	-	-

The CDA analysis reveals in general that the β-diketiminate ligand is primarily an electron donor, utilizing both σ- and π- bonding with the Ru center with strong charge transfer, which is reduced with CF_3-substitution for both the Ru^{II} and Ru^{III} species. Only a small fraction of back-donation from the metal to β-diketiminate ligand is calculated. However, an interesting observation is that the greatest back-donation occurs for complex **7**, which has a different β-diketiminate geometry compared to the other compounds. Specifically, all non-cationic Ru complexes, synthetically isolated to date, bearing bis-*ortho* substitution at the β-diketiminate

ligand feature folding at the N-N' vector. This effectively separates this allylic type N-Ru-N unit from the rest of the ligand.

The net transfer of electron density is high originating from the β-diketiminate. Comparison between the Ru^{II} and Ru^{III} highlights overall more electron transfer from all ligands to more electron deficient d^5 metal center associated with the higher oxidation state. Moreover, the halogen ligand is shown to be predominately a σ-donor with almost no back bonding capacity. The Cp* ligand is shown to be both a strong electron π-type donor, but also in the complexes presented here, an electron acceptor, displaying a significant quantity of metal to ligand back bonding identified as an interaction between the Ru(d-orbitals) and Cp* antibonding π*-type. As expected, introduction of the CF_3 group results in a reduced amount of electron transfer to the Ru center in both series of complexes, but the amount of metal to ligand back-donation is also slightly higher, which can be correlated with lowering in energy of the appropriate π*-type orbital associated with the N-C π-bonds of the β-diketiminate ligand. Also of note is the slight decrease in charge transfer from the Cp* ligand to Ru center in both **11**($Ru^{III)}$ and **17**(Ru^{II}), which is also paralleled with a slight increase in π* occupation of the Cp*. Hence, the overall net electron donation of the Cp* ligand to the Ru center is comparatively less than that provided by the β-diketiminate ligand with either CF_3 or CH_3 α-substitution. Thus the electron donating strength of β-diketiminate ligand is readily noted, which can be qualitatively verified by ESI-MS experiments which show that the Cp* fragment is readily lost before the β-diketiminate ligand under ion-trapping/fragmentation conditions for complex **7**.

S1.2: *Computational simulation of UV-visible spectra and electronic transition assignment*

Using the standard computational chemistry technique of time dependent density functional theory, TDDFT,[4] spectra for four representative complexes were modelled, which included the Ru^{III} chlorine, (Figure S1) and Ru^{II}, (Figure S2) bearing electron-donating or electron-withdrawing β-diketiminate ligands. In general the λ_{max} of absorption were shifted compared to experimental values, with the models **13** and **17** showing the best correlations, while the corresponding Ru^{III} complexes differ by several wavelengths. This larger difference partially originates from solvent effects, both Ru^{III}-Cl complexes **7** and **11** were measured in the polar solvent dichloromethane, while the experimental spectrum for the Ru^{II} complexes was obtained using n-pentane.

Importantly the TDDFT models correlate well the observed number of λ_{max}, two in the case of complexes with *ortho*-substituted β-diketiminate and three for species bearing CF_3 α-substituted β-diketiminate ligands. Assignment of the UV-visible transitions tended to be

more difficult in the case of the Ru^{III} complexes due increased orbital mixing with the various MOs, which results in multiple combinations of MLCT with d-d transitions. However, calculations correctly predict that the d-d transitions are more intense in the Ru^{III} complexes than in the Ru^{II} counterparts, although for complex **7**, the d-d transition is predicted to narrower than is experimentally observed, again the difference possibility due to solvent effects. Calculations suggest that the primary difference between the Ru^{III} and Ru^{II} complexes **7**,**11** and **13**,**17** is the increased mixing of the Ru d-orbitals with those of the Cl and β-diketiminate ligand, which causes highly broaden bands of d-d transitions. In contrast, the Ru^{II} complexes are greatly simplified, probably due to the loss of a third mixing ligand. The calculations assign the weak transitions, greater than 500 nm, to d-d transitions and strong LMCT bands. The essential difference between complexes **13** and **17** is the existence of a lower energy MLCT between Ru and the CF_3 α-substituted β-diketiminate ligand, band λ(B) (Table 3 of the main text). This correlates strongly with the contrasting character of the LUMO, where in complex **13**, it is predominately Ru-based, whereas in **17**, it is primarily based on the CF_3 α-substituted β-diketiminate (Figure S3).

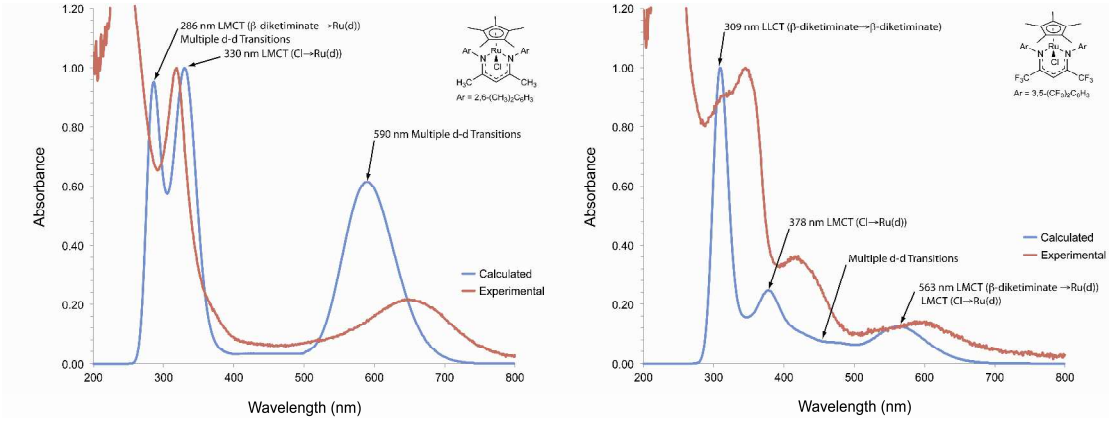

Figure S1: Comparison between experimentally obtained UV-visible spectra and TDDFT calculated UV-visible spectra for the Ru^{III} complexes **7** (left) and **11** (right). Assignments based from DFT calculation are shown.

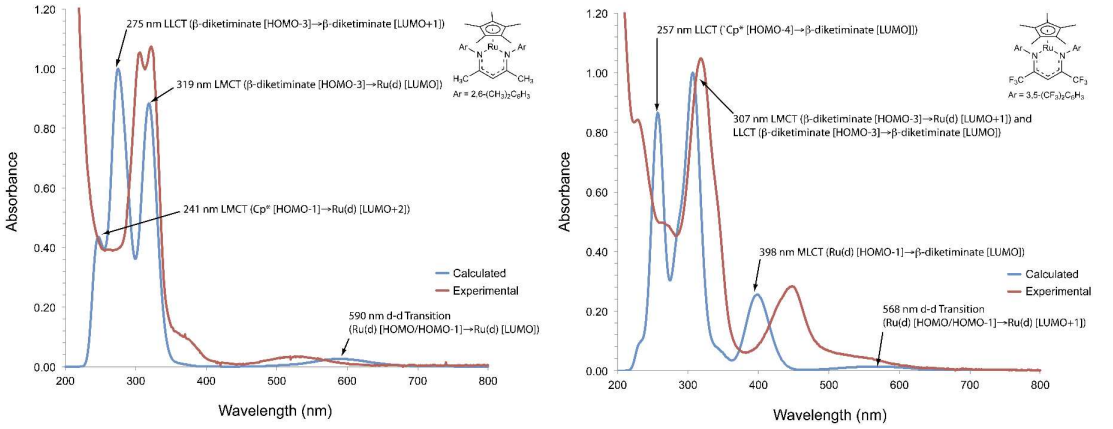

Figure S2: Comparison between experimentally obtained UV-visible spectra and TDDFT calculated UV-visible spectra for the Ru^{II} complexes **13** (left) and **17** (right). Assignments based from DFT calculation are shown.

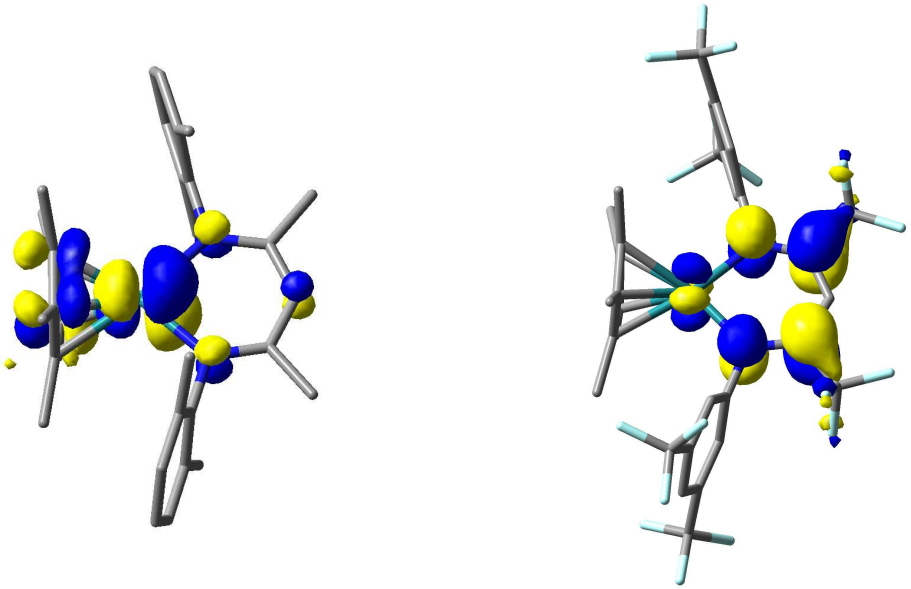

LUMO of complex **13** LUMO of complex **17**

Figure S3: Kohn-Sham DFT calculated LUMOs of complexes **13** and **17**, demonstrating the contrasting composition.

S1.3: *Specific details regarding the calculation of the model complexes*

All models were geometry optimized to an energy minimum convergence with the program Gaussian 09 subversion d,[5] using the Becke three-parameter hybrid functional (B3LYP) level of theory.[6] A 6-31G(d,p) basis set was used for non-metal atoms[7] and the quasi-relativistic Stuttgart/Dresden energy-consistent pseudo-potentials basis set (SDD-ECP) was employed for the Ru centers.[8] In all cases, the five set of pure d basis functions were used. All models represent an energy minimum on the potential energy surface as confirmed by absence of imagery (negative) frequencies, obtained through the diagonalization of the analytically computed Hessian (vibrational frequencies calculations). Atomic coordinates for all model complexes are given in Tables S4-S7. Post-population analysis, including calculation of the Mayer bond indices,[1] charge transfer fragmentation analysis was performed using the AOMIX suite of programs.[2] UV-Vis spectra were simulated with TDDFT methods[4] with calculation of the 50 first singlet states. Calculations of the corresponding triplet states were shown to be too high in energy to contribute to the spectra. Post-analysis and electronic transition assignment for UV-visible spectra was aided using the Gaussview 4.1[9] and SWizard program.[10] The LUMO diagrams in figure S3 were created with the Gaussview 4.1 program.[9]

Table S4: Atomic coordinates for the computational optimized gas phase model of the (η^5-$C_5(CH_3)_5$)RuCl(2,6-$(CH_3)_2C_6H_3NC(CH_3))_2CH$ molecule, **7**.

Atom	X	Y	Z
N	1.47625	1.02346	0.42382
C	2.79989	0.82779	0.11310
C	1.28481	2.16197	1.10092
C	3.80362	0.17820	0.63855
C	3.08765	1.34018	1.39910
C	2.46228	3.07574	1.40295
C	0.03065	2.62907	1.52043
C	5.07046	0.01242	0.05875
C	3.5818-	0.27405	2.06215
C	4.36954	1.16534	1.93153
C	2.03993	2.08478	2.19086
H	2.90157	3.47531	0.48327
H	3.25845	2.54580	1.93088
H	2.14123	3.91698	2.01904
H	0.04405	3.54155	2.10270
C	-1.23926	2.18024	1.12916
C	5.35900	0.49652	1.21404
H	5.84321	0.49272	0.63335
H	3.84814	0.52608	2.76598
H	2.54292	0.53688	2.26370
H	4.22369	1.12774	2.30080
H	4.58782	1.55957	2.92099
H	1.11956	1.50128	2.28149
H	1.75796	3.02865	1.70945
H	2.40527	2.31953	3.19455
N	-1.45316	1.04928	0.44921
C	-2.40043	3.10547	1.45733
H	6.34858	0.36060	1.64107
C	-2.77859	0.87190	0.08605
H	-2.05947	3.94026	2.07153
H	-2.85380	3.51418	0.54843
H	-3.19136	2.57974	1.99767
C	-3.06571	1.40539	1.36428
C	-3.78022	0.20984	0.65527
C	-4.34732	1.23424	1.89978
C	-2.03044	2.19710	2.12688
C	-5.05340	0.07085	0.08336
C	-3.53506	0.31055	2.05180

Atom	X	Y	Z
C	-5.34126	0.56854	1.18356
H	-4.56670	1.64271	2.88323
H	-1.81375	3.15319	1.63525
H	-1.07971	1.66328	2.19145
H	-2.37837	2.41757	3.14002
H	-5.82718	0.43864	0.65273
H	-2.49927	0.61500	2.20958
H	-3.75203	0.46133	2.80236
H	-4.19784	1.15439	2.26923
H	-6.33307	0.44480	1.60911
Ru	-0.00248	0.46505	0.21609
Cl	0.03388	0.60743	2.67335
C	0.83087	2.56250	0.08365
C	-0.61181	2.68179	0.25741
C	1.06097	1.94912	1.18293
C	1.84313	3.20115	0.98703
C	-1.24609	2.13303	0.88634
C	-1.27115	3.43217	1.37465
C	-0.22048	1.61584	1.75451
C	2.36738	1.87921	1.91396
H	1.82409	4.29338	0.87440
H	2.85524	2.86076	0.75991
H	1.63066	2.96581	2.03333
C	-2.69771	2.25026	1.24008
H	-2.34641	3.24467	1.40862
H	-1.12158	4.51121	1.23774
H	-0.84931	3.14367	2.34017
C	-0.44876	1.10405	3.14818
H	2.48230	2.78407	2.52616
H	2.42118	1.02064	2.58407
H	3.21983	1.82219	1.23672
H	-2.84591	3.14686	1.85738
H	-3.32843	2.34952	0.35663
H	-3.05830	1.39178	1.80897
H	-0.47942	1.94078	3.85981
H	-1.39822	0.57071	3.23151
H	0.34978	0.43243	3.47297

Table S5: Atomic coordinates for the computational optimized gas phase model of the (η^5-$C_5(CH_3)_5$)RuCl(3,5-$(CH_3)_2C_6H_3NC(CF_3)$)$_2$CH molecule, **11**.

Atom	X	Y	Z
N	-1.47988	0.83061	-0.47479
C	-2.83501	0.45658	-0.19278
C	-1.25376	1.90458	-1.22960
C	-3.42372	-0.58330	-0.92362
C	-3.56696	1.10568	0.80167
C	-2.43141	2.75340	-1.75245
C	-0.00001	2.39247	-1.59944
C	-4.74252	-0.94880	-0.66173
H	-2.84283	-1.07631	-1.69569
C	-4.88606	0.72195	1.05977
H	-3.11404	1.91392	1.36372
F	-3.36832	2.00533	-2.36367
F	-3.02988	3.42503	-0.74153
F	-2.03396	3.67746	-2.64635
H	-0.00002	3.26371	-2.22958
C	1.25374	1.90461	-1.22957
C	-5.48528	-0.30042	0.33011
C	-5.34585	-2.11486	-1.40044
C	-5.61352	1.38015	2.20126
N	1.47988	0.83065	-0.47475
C	2.43135	2.75346	-1.75247
H	-6.51063	-0.58788	0.52626
F	-5.05095	-3.28529	-0.77353
F	-6.69056	-2.03357	-1.46050
F	-4.87886	-2.21556	-2.65847
F	-6.93807	1.13785	2.17337
F	-5.43668	2.71783	2.20405
F	-5.14635	0.92429	3.39244
C	2.83502	0.45660	-0.19278
F	2.03383	3.67737	-2.64650
F	3.36835	2.00541	-2.36356
F	3.02970	3.42531	-0.74161
C	3.56697	1.10561	0.80173
C	3.42374	-0.58320	-0.92372
C	4.88608	0.72189	1.05977
H	3.11405	1.91378	1.36387
C	4.74254	-0.94870	-0.66189
H	2.84284	-1.07615	-1.69583
C	5.48531	-0.30039	0.33000
C	5.61355	1.37999	2.20131
C	5.34588	-2.11467	-1.40073
H	6.51067	-0.58786	0.52611
F	5.14640	0.92400	3.39245
F	6.93810	1.13772	2.17338
F	5.43668	2.71766	2.20423
F	5.05102	-3.28517	-0.77392
F	4.87888	-2.21526	-2.65875
F	6.69059	-2.03336	-1.46080
Ru	0.00000	-0.51684	0.15699
Cl	0.00005	-1.32644	-2.14854
C	-0.00003	-1.04710	2.36319
C	1.16820	-1.68507	1.80667
C	-1.16823	-1.68509	1.80662
C	-0.00007	-0.07553	3.50897
C	0.73165	-2.58983	0.80378
C	2.55295	-1.57397	2.36564
C	-0.73162	-2.58985	0.80375
C	-2.55302	-1.57401	2.36552
H	-0.00008	-0.61048	4.46809
H	0.88379	0.56687	3.49269
H	-0.88394	0.56685	3.49266
C	1.56629	-3.55363	0.01656
H	2.64619	-2.27922	3.20222
H	3.31832	-1.83324	1.63454
H	2.77494	-0.58051	2.75692
C	-1.56621	-3.55367	0.01650
H	-2.64629	-2.27925	3.20210
H	-2.77504	-0.58055	2.75679
H	-3.31835	-1.83329	1.63438
H	2.62913	-3.31288	0.05509
H	1.44003	-4.56801	0.41651
H	1.25691	-3.56462	-1.03200
H	-1.43995	-4.56804	0.41646
H	-2.62905	-3.31294	0.05498
H	-1.25679	-3.56466	-1.03205

Table S6: Atomic coordinates for the computational optimized gas phase model of the (η^5-$C_5(CH_3)_5$)Ru(2,6-$(CH_3)_2C_6H_3NC(CH_3))_2CH$ molecule, **13**.

Atom	X	Y	Z
N	1.16141	-0.01812	1.45130
C	0.75474	0.00652	2.83035
C	2.49359	-0.03103	1.25954
C	0.57748	1.24487	3.48406
C	0.57963	-1.20738	3.52799
C	3.44246	-0.02905	2.44966
C	3.10055	-0.04333	0.00000
C	0.18082	1.24538	4.82759
C	0.86685	2.54679	2.77483
C	0.19977	-1.16227	4.87455
C	0.81198	-2.53310	2.84383
H	3.28658	-0.89894	3.09445
H	3.30049	0.85440	3.07911
H	4.47871	-0.04002	2.10767
H	4.18332	-0.05429	0.00000
C	2.49359	-0.03103	-1.25954
C	-0.00806	0.05272	5.52432
H	0.03731	2.19729	5.33345
H	1.94698	2.72573	2.69738
H	0.47752	2.54012	1.75406
H	0.43404	3.39202	3.31761
H	0.06260	-2.09610	5.41451
H	0.30367	-2.57065	1.87564
H	1.87570	-2.70548	2.63866
H	0.45816	-3.36011	3.46625
N	1.16141	-0.01812	-1.45130
C	3.44246	-0.02905	-2.44966
H	-0.30997	0.07084	6.56768
C	0.75474	0.00652	-2.83035
H	4.47871	-0.04002	-2.10767
H	3.28658	-0.89894	-3.09445
H	3.30049	0.85440	-3.07911
C	0.57963	-1.20738	-3.52799
C	0.57748	1.24487	-3.48406
C	0.19977	-1.16227	-4.87455
C	0.81198	-2.53310	-2.84383
C	0.18082	1.24538	-4.82759

Atom	X	Y	Z
C	0.86685	2.54679	-2.77483
C	-0.00806	0.05272	-5.52432
H	0.06260	-2.09610	-5.41451
H	1.87570	-2.70548	-2.63866
H	0.30367	-2.57065	-1.87564
H	0.45816	-3.36011	-3.46625
H	0.03731	2.19729	-5.33345
H	0.47752	2.54012	-1.75406
H	1.94698	2.72573	-2.69738
H	0.43404	3.39202	-3.31761
H	-0.30997	0.07084	-6.56768
Ru	-0.34440	-0.01686	0.00000
C	-2.16360	-1.22300	0.00000
C	-2.22721	-0.38091	-1.17218
C	-2.22721	-0.38091	1.17218
C	-2.27999	-2.72006	0.00000
C	-2.19452	0.97417	-0.72603
C	-2.50492	-0.84671	-2.57042
C	-2.19452	0.97417	0.72603
C	-2.50492	-0.84671	2.57042
H	-3.33525	-3.02713	0.00000
H	-1.81048	-3.16060	-0.88331
H	-1.81048	-3.16060	0.88331
C	-2.37410	2.19133	-1.58527
H	-2.11972	-0.15667	-3.32258
H	-2.07074	-1.82814	-2.77120
H	-3.59025	-0.93349	-2.72106
C	-2.37410	2.19133	1.58527
H	-3.59025	-0.93349	2.72106
H	-2.07074	-1.82814	2.77120
H	-2.11972	-0.15667	3.32258
H	-3.44136	2.43701	-1.67605
H	-1.87425	3.06572	-1.15986
H	-1.98400	2.03663	-2.59323
H	-3.44136	2.43701	1.67605
H	-1.98400	2.03663	2.59323
H	-1.87425	3.06572	1.15986

Table S7: Atomic coordinates for the computational optimized gas phase model of the (η^5-$C_5(CH_3)_5$)Ru(3,5-$(CF_3)_2C_6H_3NC(CF_3))_2CH$ molecule, **17**.

Atom	X	Y	Z
N	-0.87706	-0.32369	1.45694
C	-0.45866	-0.12380	2.81666
C	-2.14717	-0.71290	1.24896
C	0.14049	-1.16044	3.53623
C	-0.64752	1.11612	3.43207
C	-3.08450	-0.99487	2.43546
C	-2.73264	-0.90468	0.00000
C	0.55112	-0.95107	4.85364
H	0.27028	-2.12844	3.06722
C	-0.23807	1.31418	4.75098
H	-1.12250	1.91791	2.87808
F	-3.29688	0.11006	3.18377
F	-2.58850	-1.95206	3.24990
F	-4.29784	-1.42472	2.03769
H	-3.75679	-1.23272	0.00000
C	-2.14717	-0.71290	-1.24896
C	0.36438	0.28514	5.47354
C	1.27364	-2.05880	5.57213
C	-0.38115	2.68743	5.35067
N	-0.87706	-0.32369	-1.45694
C	-3.08450	-0.99487	-2.43546
H	0.67924	0.44157	6.49741
F	1.26940	-1.88981	6.90863
F	2.57517	-2.11661	5.18296
F	0.73676	-3.26725	5.30540
F	0.57332	3.52533	4.87002
F	-0.25935	2.67495	6.69258
F	-1.57218	3.24510	5.04843
C	-0.45866	-0.12380	-2.81666
F	-3.29688	0.11006	-3.18377
F	-2.58850	-1.95206	-3.24990
F	-4.29784	-1.42472	-2.03769
C	-0.64752	1.11612	-3.43207
C	0.14049	-1.16044	-3.53623
C	-0.23807	1.31418	-4.75098
H	-1.12250	1.91791	-2.87808
C	0.55112	-0.95107	-4.85364

Atom	X	Y	Z
H	0.27028	-2.12844	-3.06722
C	0.36438	0.28514	-5.47354
C	-0.38115	2.68743	-5.35067
C	1.27364	-2.05880	-5.57213
H	0.67924	0.44157	-6.49741
F	-0.25935	2.67495	-6.69258
F	-1.57218	3.24510	-5.04843
F	0.57332	3.52533	-4.87002
F	1.26940	-1.88981	-6.90863
F	2.57517	-2.11661	-5.18296
F	0.73676	-3.26725	-5.30540
Ru	0.55567	0.03508	0.00000
C	2.04985	1.62608	0.00000
C	2.31510	0.82373	-1.17214
C	2.31510	0.82373	1.17214
C	1.78660	3.10349	0.00000
C	2.58519	-0.50441	-0.72628
C	2.50148	1.36291	-2.55835
C	2.58519	-0.50441	0.72628
C	2.50148	1.36291	2.55835
H	2.73048	3.66546	0.00000
H	1.22103	3.40895	-0.88385
H	1.22103	3.40895	0.88385
C	3.00736	-1.67567	-1.56469
H	2.37558	0.59598	-3.32326
H	1.81969	2.18368	-2.78702
H	3.52279	1.75513	-2.65577
C	3.00736	-1.67567	1.56469
H	3.52279	1.75513	2.65577
H	1.81969	2.18368	2.78702
H	2.37558	0.59598	3.32326
H	4.09696	-1.80202	-1.50984
H	2.55592	-2.60694	-1.20969
H	2.74826	-1.55303	-2.61672
H	4.09696	-1.80202	1.50984
H	2.74826	-1.55303	2.61672
H	2.55592	-2.60694	1.20969

S1.4: *Description of Solid State Packing for Complexes **7-11** and **13-17***

Ru^{II} and Ru^{III} complexes bearing β-diketiminate ligand with a CF_3 substitution either at the flanking aryl or α-position, show a tendency to maximize fluorine-fluorine interactions, which ranged from 2.773 to 2.838 Å, (Table S8), some representative examples are shown in Figures S4-6. For those structures, featuring solvates, the intra-molecular interacts are confined to non-fluorinated regions of the main complex (Figure S6). Interestingly, for the Ru^{II} series of compounds, the closest inter-molecular contacts are between hydrogen atoms. In the case of complex **7**, the strong nucleophilicity of the β-carbon site can be observed as a strong inter-molecular contact with the hydrogen atom of a nearby α-CH_3 group, (Figure S7). For the majority of complexes, both Ru^{III} and Ru^{II}, face-to-face orientation of the Cp* group is observed, *i.e.*, complex **13**, (Figure S8). However, a slight change in the substitution pattern of the flanking aryl, i.e. 2,6-dimethyl (**13**) versus 3,5-dimetly (**14**) causes a stacking arrangement between aryl group and the Cp* ligand (Figure S9).

Table S8: Selected intra-molecular distances for Ru^{III} complexes **7-11** and Ru^{II} **13-17** complexes.

Complex	Ar	α-CR_3	Shortest Intermolecular H···X Interaction (Å)	Intermolecular H···Cl Interaction (Å)	Shortest Intermolecular F···F Interaction (Å)
7	2,6-$(CH_3)_2C_6H_3$	CH_3	2.786 X = C	2.935	-
8	3,5-$(CH_3)_2C_6H_3$	CH_3	2.552 X = C	2.833	-
9	3,5-$(CF_3)_2C_6H_3$	CH_3	2.323 X = H	2.711	-
10	3,5-$(CH_3)_2C_6H_3$	CF_3	2.525 X =F	-	2.773
11	3,5-$(CF_3)_2C_6H_3$	CF_3	2.388 X = F	2.791	2.820
13	2,6-$(CH_3)_2C_6H_3$	CH_3	2.317 X = H	-	-
14	3,5-$(CH_3)_2C_6H_3$	CH_3	2.391 X = H	-	-
15	3,5-$(CF_3)_2C_6H_3$	CH_3	2.380 X = H	-	2.826
16	3,5-$(CH_3)_2C_6H_3$	CF_3	2.378 X =H	-	2.769
17	3,5-$(CF_3)_2C_6H_3$	CF_3	2.344 X = H	-	2.838

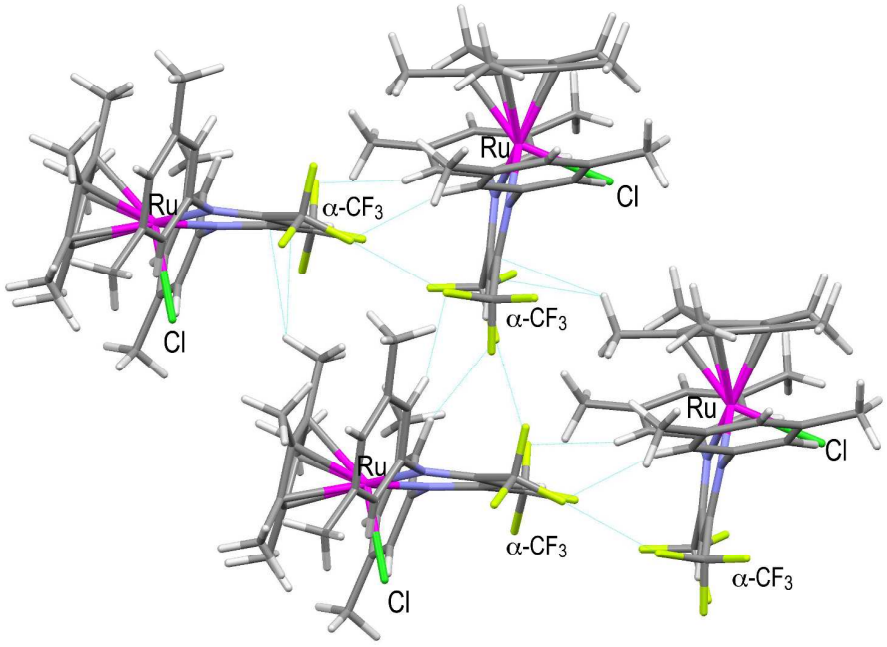

Figure S4: Solid-state crystal packing ball and stick diagram of complex **10**, (η^5-$C_5(CH_3)_5$)RuCl(3,5-$(CH_3)_2C_6H_3NC(CF_3)$)$_2$CH, highlighting the fluorophilic interactions.

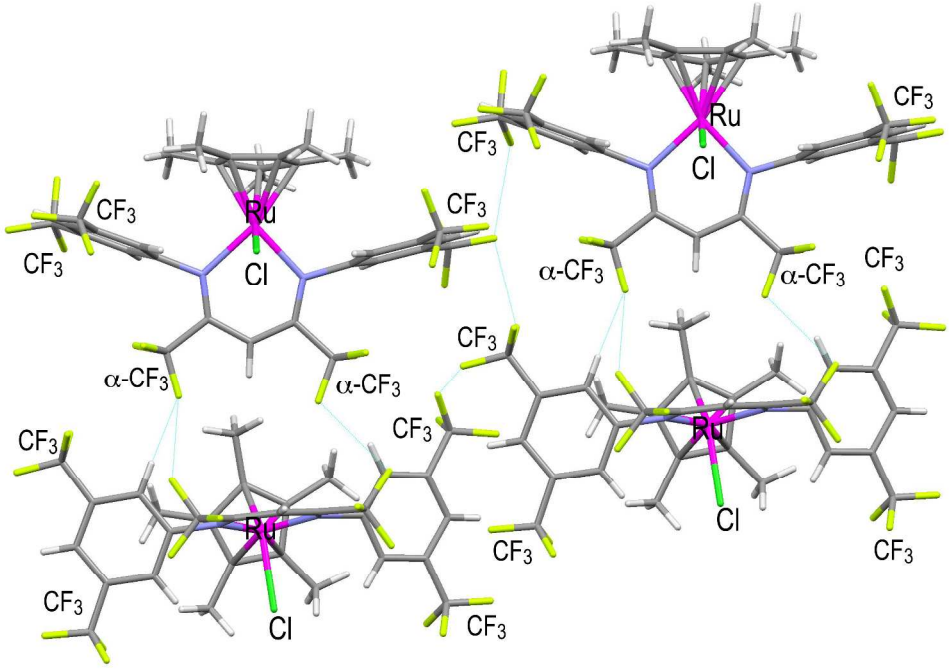

Figure S5: Solid-state crystal packing ball and stick diagram of complex **11**, (η^5-$C_5(CH_3)_5$)RuCl(3,5-$(CF_3)_2C_6H_3NC(CF_3))_2$CH, highlighting the fluorophilic interactions.

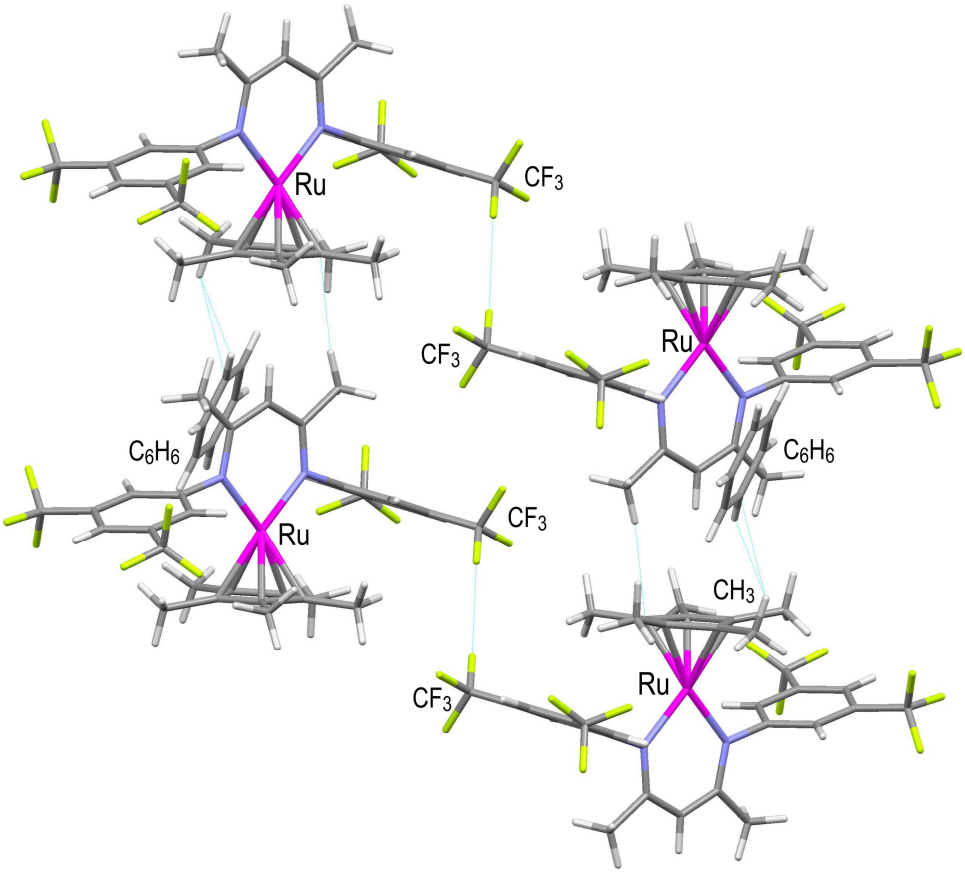

Figure S6: Solid-state crystal packing ball and stick diagram of complex **15**, (η^5-$C_5(CH_3)_5$)RuCl(3,5-$(CF_3)_2C_6H_3NC(CH_3))_2$CH, highlighting the fluorophilic interactions.

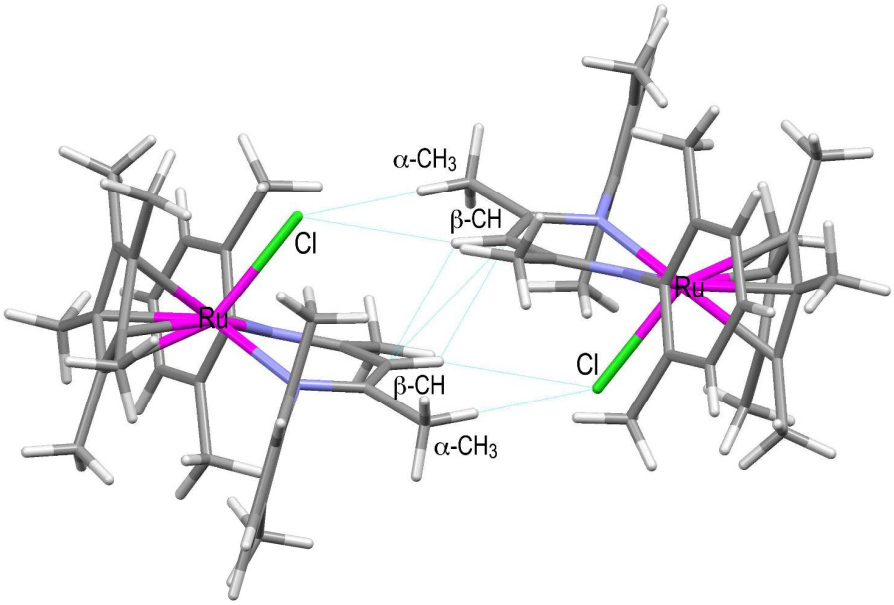

Figure S7: Solid-state crystal packing ball and stick diagram of complex **7**, (η^5-$C_5(CH_3)_5$)RuCl(2,6-$(CF_3)_2C_6H_3NC(CH_3))_2CH$, highlighting the intermolecular interactions between the α-CH_3 hydrogen and the β-carbon site.

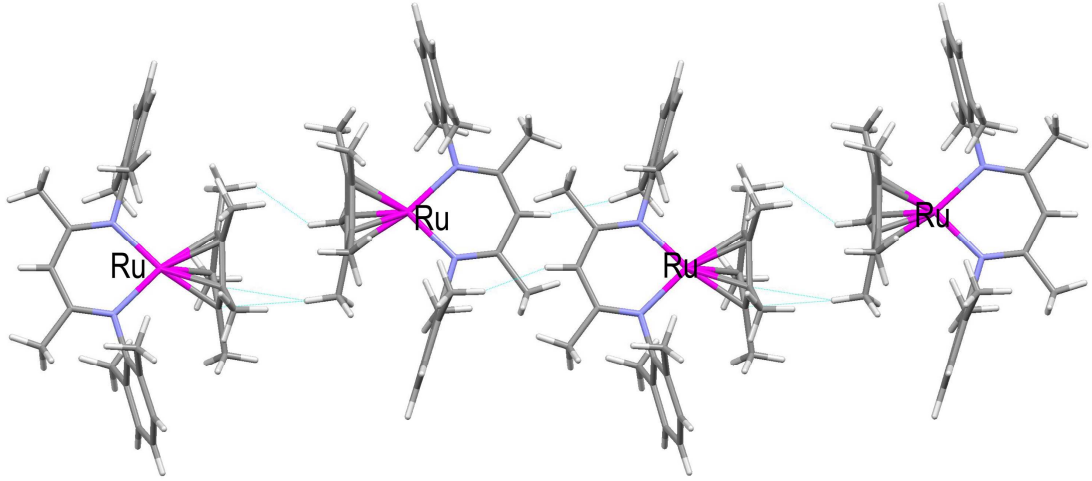

Figure S8: Solid-state crystal packing ball and stick diagram of complex **13**, (η^5-$C_5(CH_3)_5$)Ru(2,6-$(CF_3)_2C_6H_3NC(CH_3))_2CH$, highlighting the face-to-face intermolecular interactions between the Cp* ligands.

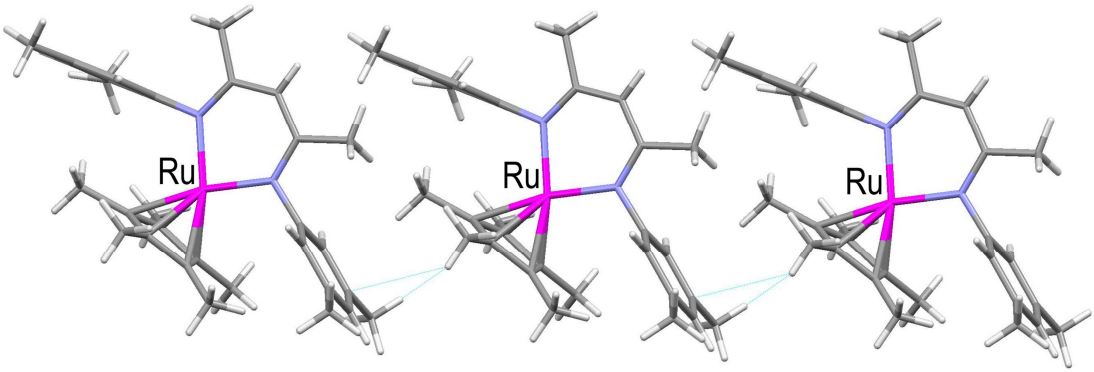

Figure S9: Solid-state crystal packing ball and stick diagram of complex **14**, (η^5-$C_5(CH_3)_5$)Ru(3,5-$(CF_3)_2C_6H_3NC(CH_3))_2CH$, highlighting the intermolecular interactions between Cp* ligand and flanking *N*-aryl groups.

S1.5: *Experimental crystallographic details*

Suitable single crystals were removed from the sample vial under a flow of N_2 and manipulated in a perfluoropolyalkylether oil-based matrix, F06206K, purchased from the ABCR company, in a special constructed Dewar partially filled with liquid nitrogen. The crystals were mounted to either end of a glass fibre (diameter 0.01 mm) or in a nylon loop attached to a metal pin affixed to a goniometer head, which was placed in the instrument while maintaining a blanket of N_2 gas. For structures **8**, **12** – **15** and **17**, a Burker-Nonius KappaCDD diffractometer equipped with an Apex II CCD area detector and an Enraf FR590 X-ray generator (50 kV, 40 mA) was used, for **9** – **11** and **16**, an Oxford-Kuma Xcalibur diffractometer with a Sapphire CCD area detector, and an Oxford Diffraction Supernova with an Atlas CCD area detector was employed in the case of structure **11**. The instruments utilize either a graphite-momochromotated Mo-Kα radiation source with λ = 0.71073 Å or Cu-Kα radiation source with λ = 1.54184 Å. The crystal was kept under a gaseous flow of N_2, with a temperature of -130 or -170 ºC during the entire collection procedure. The unit cell and orientation matrix was determined by indexing reflections measured from phi scans and analysed with the program DIRAX[11] or CrysAlis Pro.[12] All data collections were performed by scanning reflections from the entire Ewald sphere using CollectCCD[13] or CrysAlis Pro.[12] After data integration, a multi-scan absorption correction based on a semi-empirical method was applied using the SADABS[14] or the Scalepack 3 program an integrated algorithm as part of the CrysAlis Pro program.[12] Space group determination was performed with the XPREP program.[15] Structure solutions were obtained based on the direct-method algorithm executed with the programs Shelx-XS[16] or SIR-2002.[17] Afterwards, anisotropic refinement of all non-hydrogen atoms was completed based on a least-squares full-matrix method against F^2 data using exclusively Shelx-XL.[16] Hydrogen atoms were added through geometrical calculation positions and refined as a riding model using a scaled thermal parameter of the connecting atom. In cases of disorder, a split refinement model was employed for the affected atoms and the site occupation factors refined. Moreover, for some structures, bond distance and angle

restraints were introduced particularly for disordered CF_3 groups. Specific details are provided in the individual CIF files available as supporting information. A small number of reflections in some cases were removed when $\Delta(F_o^2-F_c^2)$/esd exceeded 10.0. Selected crystallographic data is given in Tables 10, 11 and 12. Drawings were created using the programs ORTEP-3 for windows[18] or CCDC Mercury.[19]

Table S9: Selected crystallographic data for Ru^{III} complexes **7** – **11**.

Parameter	**7**	**8**	**9**[a]	**10**	**11**
Empirical formula	$C_{31}H_{40}ClN_2Ru$	$C_{31}H_{40}ClN_2Ru$	$C_{31}H_{34}ClF_6N_2Ru$	$C_{31}H_{28}ClF_{12}N_2Ru$	$C_{31}H_{22}ClF_{18}N_2Ru$
Fwt (g mol^{-1})	577.17	577.17	658.12	793.07	901.03
Cryst syst.	Monoclinic	Monoclinic	Monoclinic	Orthorhombic	Monoclinic
Space Group	$P2_1/c$	$P2_1/c$	$P2_1/c$	$Pca2_1$	$P2_1$
a (Å)	11.4115(13)	15.0996(17)	12.6771(7)	30.7359(4)	13.3368(12)
B (Å)	16.1565(7)	8.1612(8)	8.2347(5)	27.2804(3)	8.1933(7)
c (Å)	16.810(2)	24.661(3)	30.471(2)	15.0300(2)	15.5139(16)
α (°)	90	90	90	90	90
β (°)	115.569(8)	115.246(9)	110.430(5)	90	102.811(10)
γ (°)	90	90	90	90	90
V ($Å^3$)	2795.7(5)	2748.7(5)	2980.8(3)	12602.5(3)	1653.0(3)
Z	4	4	4	16	2
D_{calcd} (g cm^{-3})	1.371	1.395	1.527	1.672	1.810
Radiation Type	Mo-Kα	Mo-Kα	Mo-Kα	Mo-Kα	Cu-Kα
Cryst dimens. (mm^3)	0.30 × 0.24 × 0.09	0.343 × 0.283 × 0.189	0.378 × 0.168 × 0.106	0.32 × 0.26 × 0.24	0.325 × 0.119 × 0.090
Temp. (K)	100(2)	133(2)	100(2)	100(2)	133(2)
μ (mm^{-1})	0.678	0.690	0.677	0.679	0.684
θ min./max. range (°)	3.59 / 25.00	2.85 / 24.99	2.86 / 25.00	2.62 / 25.00	2.83 / 25.00
Completeness θ (%)	99.7	99.8	99.8	99.8	99.8
F(000)	1204	1204	1396	6352	890
No. of rflns collected	51313	17514	21857	102336	12795
No. of unique rflns	4894	4834	5224	21963	5765
No. of parameters	327	327	379	1780	512
No. of restraints	0	6	0	83	25
R_1 /wR_2 ($I>2\sigma(I)$)[b]	0.0315/0.0529	0.0415/0.0734	0.0446/0.060	0.0342/0.0740	0.0602/0.1182
R_1 / wR_2 (all data)[b]	0.0541/0.0591	0.1019/0.0835	0.0887/0.1070	0.0401/0.0772	0.1055/0.1321
GOF[c]	1.103	0.842	0.942		0.950
Max./min. e^- density (e $Å^{-3}$)	0.367/-0.413	0.954/-0.573	1.324/-1.310	0.649/-0.599	2.656/-0.460
Abs. Struct.				0.00(2)	0.07(5)

(a) Four crystallographic independent molecules present within the unit cell. (b) $R_1 = \Sigma||F_o|- |F_c||/\Sigma|F_o|$, $wR_2 = \{\Sigma[w(F_o^2-F_c^2)^2] / \Sigma[w(F_o^2)^2]\}^{½}$. (c) GOF = $\{\Sigma[w(F_o^2-F_c^2)2] / (n-p)\}^{½}$ where n is the number of data and p is the number of parameters refined.

Table S10: Selected crystallographic data for Ru^{II} complexes **13** – **17**.

Parameter	**13**[a]	**14**	**15**	**16**	**17**[a]
Empirical formula	$C_{31}H_{40}N_2Ru$	$C_{31}H_{40}N_2Ru$	$C_{37}H_{34}F_{12}N_2Ru$	$C_{37}H_{28}F_{18}N_2Ru$	$C_{37}H_{40}F_6N_2Ru$
Fwt (g mol^{-1})	541.72	541.72	835.73	943.68	727.78
Cryst syst.	Triclinic	Triclinic	Triclinic	Monoclinic	Triclinic
Space Group	*P*-1	*P*-1	*P*-1	*P* $2_1/c$	*P*-1
a (Å)	11.1867(12)	9.6289(14)	8.8692(7)	8.7701(14)	9.8077(10)
B (Å)	15.6006(17)	11.0346(18)	9.2206(8)	39.424(4)	11.4136(8)
c (Å)	17.0345(13)	13.8160(15)	21.5339(17)	23.119(4)	16.3247(15)
a (°)	96.753(6)	79.105(11)	86.320(7)	90	105.494(6)
b (°)	103.186(8)	76.564(9)	87.252(7)	111.995(14)	97.740(7)
g (°)	104.813(8)	73.919(10)	85.375(7)	90	105.622(9)
V ($Å^3$)	2749.0(5)	1359.7(3)	1750.1(2)	7411.7(19)	1653.4(3)
Z	4	2	2	8	2
D_{calcd} (g cm^{-3})	1.309	1.323	1.586	1.691	1.462
Radiation type	Mo-Kα	Mo-Kα	Mo-Kα	Mo-Kα	Mo-Kα
Cryst dimens. (mm^3)	0.459 × 0.208 × 0.142	0.380 × 0.320 × 0.166	0.15 × 0.24 × 0.31	0.553 × 0.290 × 0.210	0.568 × 0.225 × 0.160
Temp. (K)	100(2)	100(2)	133(2)	100(2)	100(2)
m (mm^{-1})	0.591	0.597	0.542	0.545	0.537
θ min./max. range (°)	3.35 / 25.00	3.30 / 25.00	2.83 / 25.00	3.37 / 25.00	3.39 / 25.00
Completeness θ (%)	99.5	99.7	92.6	98.5	99.6
F(000)	1136	568	844	3760	748
No. of rflns collected	51833	26496	11896	88177	31566
No. of unique rflns	9641	4772	5696	12869	5820
No. of parameters	635	318	495	1095	424
No. of restraints	0	0	12	26	0
R_1 /wR_2 ($I>2s(I)$)[b]	0.0336/0.0600	0.0191/0.0467	0.0549/0.1147	0.0651/0.1327	0.0229/0.0532
R_1 / wR_2 (all data)[b]	0.0544/0.0677	0.0214/0.0482	0.0928/0.1241	0.0775/0.1380	0.0268/0.0551
GOF[c]	1.105	1.091	0.956	1.235	1.154
Max./min. e^- density (e $Å^{-3}$)	0.361/-0.432	0.347/-0.311	0.992/-0.519	1.300/-1.091	0.359/-0.353

(a) Two crystallographic independent molecules present within the unit cell. (b) $R_1 = \Sigma||F_o|- |F_c||/\Sigma|F_o|$, $wR_2 = \{\Sigma[w(F_o^2-F_c^2)^2] / \Sigma[w(F_o^2)^2]\}^{½}$. (c) GOF = $\{\Sigma[w(F_o^2-F_c^2)2] / (n-p)\}^{½}$ where *n* is the number of data and *p* is the number of parameters refined.

S1.6: *References*

1. (a) Mayer, I. *Theor. Chim. Acta* **1985**, *67*, 315-322. (b) Mayer, I. *Int. J. Quantum Chem.* **1986**, *29*, 73. (c) Mayer, I. Int. J. Quantum Chem. **1986**, *29*, 477. (d) Fliszár, S. *Atomic Charges, Bond Properties, and Molecular Energies*, **2008**, John Wiley & Sons, Inc.: 93-97.
2. (a) *AOMix: Program for Molecular Orbital Analysis*; Gorelsky, S. I.; University of Ottawa, Ottawa, Canada, **2011**, http://www.sg-chem.net/. (b) Gorelsky, S. I.; Lever, A. B. P. *J. Organomet. Chem*. **2001**, *635*, 187-196.
3. (a) Dapprich, S.; Frenking, G. J. Phys. Chem. **1995**, *99*, 9352-9362. (b) Frenking, G.; Frohlich, N. *Chem. Rev*. **2000**, *100*, 717-774.
4. (a). Scalmani, G.; Frisch, M. J.; Mennucci, B.; Tomasi, J.; Cammi, R.; Barone, V.; *J. Chem. Phys.* **2006**, 124, 1-15. (b) Furche, F.; Ahlrichs, R. *J. Chem. Phys.* **2002**, *117* 7433-47. (c) Van Caillie C.; Amos, R. D. *Chem. Phys. Lett.* **2000**, 317, 159-64.
5. *Gaussian 09, Revision A.1*; Frisch, M. J.; Trucks, G. W.; Schlegel, H. B.; Scuseria, G. E.; Robb, M. A.; Cheeseman, J. R.; Scalmani, G.; Barone, V.; Mennucci, B.; Petersson, G. A.; Nakatsuji, H.; Caricato, M.; Li, X.; Hratchian, H. P.; Izmaylov, A. F.; Bloino, J.; Zheng, G.; Sonnenberg, J. L.; Hada, M.; Ehara, M.; Toyota, K.; Fukuda, R.; Hasegawa, J.; Ishida, M.; Nakajima, T.; Honda, Y.; Kitao, O.; Nakai, H.; Vreven, T.; Montgomery, Jr., J. A.; Peralta, J. E.; Ogliaro, F.; Bearpark, M.; Heyd, J. J.; Brothers, E.; Kudin, K. N.; Staroverov, V. N.; Kobayashi, R.; Normand, J.; Raghavachari, K.; Rendell, A.; Burant, J. C.; Iyengar, S. S.; Tomasi, J.; Cossi, M.; Rega, N.; Millam, N. J.; Klene, M.; Knox, J. E.; Cross, J. B.; Bakken, V.; Adamo, C.; Jaramillo, J.; Gomperts, R.; Stratmann, R. E.; Yazyev, O.; Austin, A. J.; Cammi, R.; Pomelli, C.; Ochterski, J. W.; Martin, R. L.; Morokuma, K.; Zakrzewski, V. G.; Voth, G. A.; Salvador, P.; Dannenberg, J. J.; Dapprich, S.; Daniels, A. D.; Farkas, Ö.; Foresman, J. B.; Ortiz, J. V.; Cioslowski, J.; Fox, D. J. Gaussian, Inc., Wallingford CT, **2009**.
6. Becke, A. D. *J. Chem. Phys.* **1993**, *98*, 5648.
7. Petersson, G. A.; Al-Laham, M. A. *J. Chem. Phys.* **1991**, *94*, 6081.
8. Andrae, D.; Haeussermann, U.; Dolg, M.; Stoll, H.; Preuss, H. *Theor. Chim. Acta* **1990**, *77*, 123-41.
9. *GaussView, Version 4.1*; Dennington, R.; Keith, T.; Millam, J. Semichem Inc., Shawnee Mission KS, **2009**.
10. *SWizard program*; Gorelsky, S. I. University of Ottawa, Ottawa, Canada, **2011**, http://www.sg-chem.net/.
11. Duisenberg, A. J. M., *J. Appl. Cryst.* **1992**, *25*, 92-96.

12. *CrysAlis Pro*, 1.71. Agilent Technologies: Yarnton, Oxfordshire, **2011**.
13. Duisenberg, A. J. M.; Kroon-Batenburg, L. M. J.; Schreurs, A. M. M., *J. Appl. Cryst.* **2003**, *36*, 220-229.
14. Sheldrick, G. M. *SADABS. Area detector absorption and other corrections, 2.06;* Bruker-AXS: Madison, Wisconsin (USA), **2003**.
15. Sheldrick, G. M. *XPREP, A Reciprocal Space Exploration Program*, 2.06; Bruker-AXS: Madison, Wisconsin, United States, **2003**.
16. Sheldrick, G. M., *Acta Cryst A* **2007**, *64*, 112-122.
17. Burla, M. C.; Camalli, M.; Carrozzini, B.; Cascarano, G. L.; Giacovazzo, C.; Polidori, G.; Spagna, R., *J. Appl. Cryst.* **2003**, *36*, 1103.
18. Farrugia, L. J., *J. Appl. Cryst.* **1997**, *30*, 565.
19. Macrae, C. F.; Edgington, P. R.; McCabe, P.; Pidcock, E.; Shields, G. P.; Taylor, R.; Towler, M.; van de Streek, J., *J. Appl. Cryst.* **2006**, *39*, 453-457.